Available online at www.sciencedirect.com
SCIENCE DIRECT®
Journal of Magnetic Resonance 158 (2002) 178–182
JMR Journal of Magnetic Resonance
www.academicpress.com

Note

3D MR microscopy with resolution 3.7 μm by 3.3 μm by 3.3 μm

L. Ciobanu, D.A. Seeber, and C.H. Pennington*

Department of Physics, Ohio State University, 2030 Smith Labs, 174 West 18th Avenue, Columbus, OH 43210-1016, USA

Received 6 May 2002; revised 18 July 2002

Abstract

The technique of magnetic resonance imaging microscopy holds promise of bringing the full capabilities of NMR to arbitrarily specified positions within spatially inhomogeneous systems, including biological cells, yet the possibilities are limited by the need for adequate sensitivity and spatial resolution. We report proton magnetic resonance images obtained by combining advances in receiver coil sensitivity, gradient strength, and pulse/gradient sequence design. We achieve resolution of $3.7 \pm 0.4\,\mu m$ by $3.3 \pm 0.3\,\mu m$ by $3.3 \pm 0.3\,\mu m$ for a volume resolution ~ 40 femtoliters (corresponding to $\sim 3 \times 10^{12}$ proton spins).

PACS: 76.60; 87.61

Keywords: MR microscopy; MRI microscopy; Micron resolution

1. Introduction

Magnetic resonance imaging (MRI) microscopy [1] has the potential to bring the full capabilities of NMR to arbitrarily specified localized positions within small samples. The most interesting target of study is the living biological cell, with typical dimensions $\sim 100\,\mu m$, but with substructures that are much smaller, such as the cell nucleus (typically $\sim 10\,\mu m$) and mitochondria (1–10 μm). One anticipates that the development of MR microscopy with resolution at the level of these substructures or better and with a wide, three-dimensional field-of-view could open a new avenue of investigation into the biology of the living cell.

Although the first MR image of a single biological cell was reported in 1987, [2] the cell imaged had quite large (~ 1 mm diameter) spatial dimensions and the resolution obtained (on the order of 10 μm in-plane) was not adequate for meaningful imaging of more typically sized cells. The quest for higher resolution though has continued. In 1989, Zhou et al. [3] obtained fully three-dimensional spatial resolution of $(6.37\,\mu m)^3$, or $260\,(\mu m)^3$ (260 femtoliters). While better "in-plane" resolutions (i.e., the resolution in 2 of the 3 spatial dimensions) have since been obtained, [4,5] this volume resolution was not exceeded until quite recently by Lee et al. [6] who report 2D images having volume resolution $75\,\mu m^3$ and in-plane resolution of 1 μm. In parallel with these advances in raw resolution several investigators [7–9] have focused on localized spectroscopy and/or chemical shift imaging.

2. Results

The key obstacles to overcome in MR microscopy are (1) the loss of signal-to-noise that occurs when observing small volumes and (2) molecular diffusion during the measurement or encoding. To date the problem of sensitivity has typically been addressed by employing small micro-coil receivers [10]. The problem of molecular diffusion can only be defeated with strong magnetic field gradients that can encode spatial information quickly. In recent technical publications [11–13] we presented approaches to these obstacles. Specifically we detailed our development of a triaxial gradient system [12] capable of producing gradients as large as 50 T/m (5000 G/cm) and our micro-coil circuitry setup [11] for attaining high sensitivity.

* Corresponding author. Fax: 614-292-7557.
E-mail address: penningt@mps.ohio-state.edu (C.H. Pennington).

1090-7807/02/$ - see front matter © 2002 Elsevier Science (USA). All rights reserved.
PII: S1090-7807(02)00071-X

Here we report an MR microscopy image obtained using these apparati. The image has resolution of ($3.7 \pm 0.4\,\mu m$ by $3.3 \pm 0.3\,\mu m$ by $3.3 \pm 0.3\,\mu m$), or $\sim 40\,\mu m^3$ ($\sim$40 femtoliters, containing $\sim 3 \times 10^{12}$ proton spins), marginally the highest voxel resolution reported to date. (Images are taken at room temperature and 9 T.) The image has not only excellent resolution, but also a wide, fully three-dimensional field-of-view ($237\,\mu m$ by $66\,\mu m$ by $66\,\mu m$ in this case), which can provide context and perspective that is lacking in 2D images.

This combination of high sensitivity, resolution, and field-of-view accrued not only from using micro-coils and strong gradients, but also from two other factors inherent in the "constant-time-imaging" [14,15] scheme employed. Briefly (see Section 5 for detail), we apply a spin-echo sequence, phase-encoding in all three spatial dimensions; this is followed by a CP or CPMG train to enhance signal-to-noise. First, we benefit from the use of non-selective excitation pulses, whereby for each recycle delay we acquire signal from the entire 3D sample. Given the need for high resolution and for many averaging scans, one obtains, as a fortuitous by-product, a wide field-of-view. Conversely, given a need for wide field-of-view, higher sensitivity, and signal-to-noise accrues in each voxel. Second, the CP re-focusing trains are applied in the absence of gradients, nicely narrowing the effective bandwidth of the signal and increasing signal-to-noise.

The sample, shown in Fig. 1, is a quartz micro-capillary filled with water and packed $39 \pm 4\,\mu m$ diameter fluorescent polymer beads forming a crooked single-file column. (The $\sim$10% uncertainty in bead diameter carries over to all length scales reported here, including resolution, and henceforward we will suppress it.) The water provides the observed NMR signal. The water contained 0.01 M cupric nitrate, shortening T_1 to $\sim$350 ms, typical of biological samples [1]. The NMR receiver coil (Fig. 2) is wound upon the micro-pipette and tuned, and the sample with tuned circuit is mounted within the gradient coil platform, all as described in [11–13].

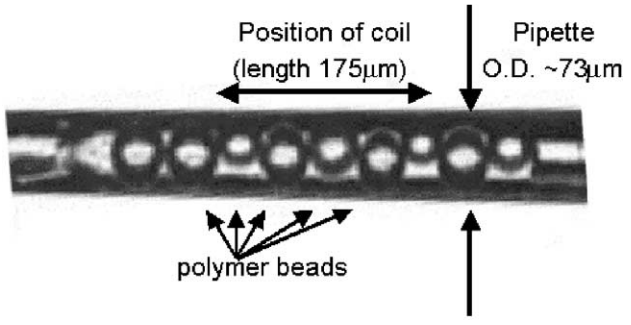

Fig. 1. Microscope photograph of the sample imaged, a quartz micro-capillary, initially 1 mm OD, pulled to an OD of $\sim$73 μm and ID $\sim$53 μm, filled with water and $39 \pm 4\,\mu m$ diameter fluorescent polymer beads (Duke Scientific). Proton linewidth was 200 Hz FWHM. Fig. 2 shows this same sample with the rf micro-coil wound upon it.

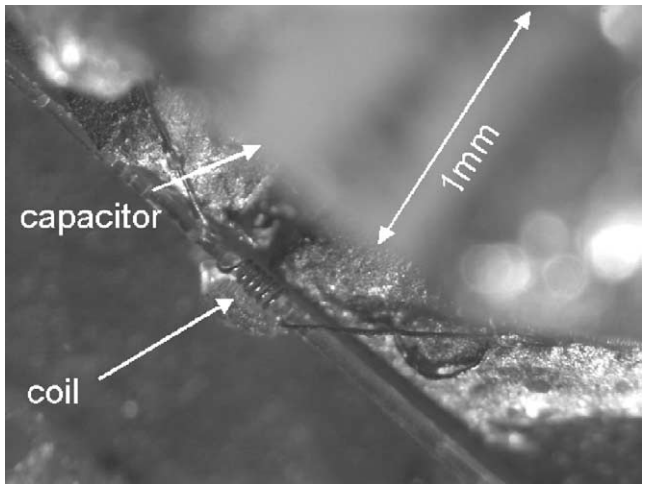

Fig. 2. The sample of Fig. 1 with the rf micro-coil applied. The micro-coil has 6 turns of 20 μm copper wire with a total length $\sim$175 μm and inner diameter $\sim$73 μm. Beads outside of the coil are visible in the figure. Also visible, though out of focus, is a 56 pf capacitor that tunes the rf coil at 383 MHz.

The resulting 3D magnetic resonance image of this sample is shown in Fig. 3. Given in successive panels are 25 (out of a total of 32) XY plane slices, with the X direction defined as parallel to the axis of the micro-pipette, and with the Z-direction vertical and parallel to the applied magnetic field. The Y direction is horizontal and perpendicular to the micro-pipette axis. The image plainly shows the key features of the 39 μm diameter beads-in-capillary sample. It confirms, for example, that the beads are typically displaced, both along the Y and Z axes, from the central axis of the micro-pipette. In slices near the central axis of the pipette we plainly observe each of the five beads that are inside the receiver coil. Slices far from the central axis, however, typically show only one or two beads—the ones that are displaced from the center in the corresponding direction.

3. Assessment of resolution

It is expected (see Section 5) that the resolution attained using the "constant-time-imaging" [14,15] sequence will be equal to that calculated based solely on the widths of the region of $\vec{k}$-space sampled, without T_2 or susceptibility broadening artifacts. That resolution, the "nominal" resolution, along X (Y) [Z], based on the phase-encoding parameters used here (see Section 5) is 3.7 μm (3.3 μm) [3.3 μm]. Fig. 4a–c presents image slices displaying sharp features that we use to assess the actual resolution along, respectively, the X, Y, and Z directions.

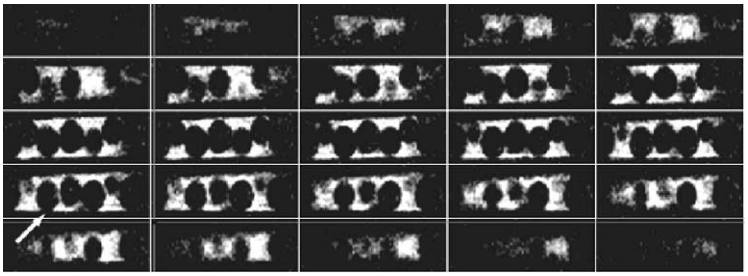

Fig. 3. 3D MRI microscopy image of the sample of Fig. 1, containing water and ~39 μm fluorescent polymer beads. Defining the X direction as the axis of the pipette and Z the axis of the applied field, the image shown consists of 25 (of a total of 32) XY plane slices of thickness 2.06 μm. In-plane voxel widths along X (Y) are 3.7 μm (2.06 μm). The resolution expected (and assessed below) along X (Y) [Z], based on the widths of the region sampled in $\vec{k}$ space, is 3.7 μm (3.3 μm) [3.3 μm]. (Zero-filling is applied along Y and Z, taking the array widths from 20 to 32 points and resulting in smaller voxel widths [2.06 μm] for these directions. The actual resolution is of course unaffected.) Image is taken at room temperature at a field of 9 T (383 MHz). Signal-to-noise (signal amplitude in regions where water is present divided by the rms noise in regions without water) is ~5. A total of 204,800 echo trains were acquired, with recycle delay of order of the spin lattice relaxation time T_1 (350 ms), for a total acquisition time of ~30 h. The white arrow indicates the slice that is pictured in Fig. 4a.

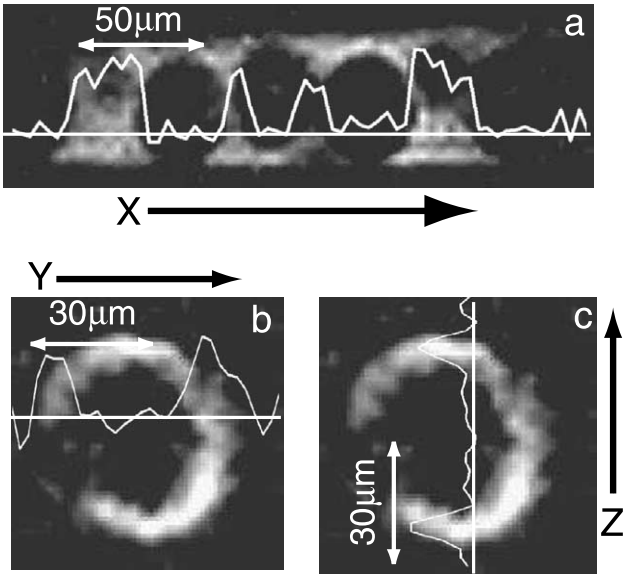

Fig. 4. Image slices in the XY (a) and YZ (b and c) plane. Superposed on each image is a plot of signal vs. X (in panel a) for constant Y and Z. Analogous plots for Y and Z are given in (b) and (c). Slice thickness is 2.06 μm (a) and 3.7 μm (b) and (c). The plots display sharp edge features that are magnified and displayed in Fig. 5 to assess resolution.

Fig. 4a shows an XY slice, specifically the one labeled by a white arrow in Fig. 3. Marked in Fig. 4a is a region of width 50 μm that includes an "edge" feature in which the signal amplitude drops from essentially full strength (corresponding to 100% water concentration) to zero. The signal in that 50 μm region is then plotted with a magnified view vs. X (for constant values of Y and Z) in Fig. 5a. Fig. 5a shows that the edge-feature, the drop from full strength to zero, occurs over one voxel width of 3.7 μm, confirming the expected resolution of 3.7 μm [16].

We assess the Y and Z resolutions analogously. Figs. 4b, c and 5b, c demonstrate that for edge features along Y and Z, the signal intensity drops from 100% to near zero over a distance comparable to our expected resolution of ~3.3 μm.

4. Discussion

This work demonstrates some impressive possibilities available through the combination of micro-coil receivers, strong gradients, and pulsing schemes designed to maximize signal-to-noise. We attain very high resolution and a correspondingly small number (3×10^{12}) of protons detected at this field and temperature, comparing favorably with that attained in magnetic resonance force microscopy (MRFM) (Schaff et al. [17] report a MRFM requiring $\sim 10^{13}$ protons for signal-to-noise 1 on a single scan; from data presented here we find that our instrument requires $\sim 4.9 \times 10^{13}$. Our set-up, however, averages on the entire sample with each scan, while the MRFM must scan point-by-point in real-space, accumulating signal from just one voxel at a time.). However, the limitations of the approach are also apparent. The ~3 μm resolution attained would appear to provide a good length scale for cell applications. This resolution, though, is only attained for protons in water at full concentration of 55 mol/l. The prospect for detection of other organic molecules at much lower concentrations at this resolution appears daunting. (Furthermore the CP scheme used here discards chemical shift information. CP would be less necessary if measures were taken to narrow the inhomogeneous linewidth [18].) An additional problem is of course the long time (~30 h) required for the image.

Most likely the advantages of micro-coil MR will be best realized in experiments seeking richer information at less aggressive resolutions. Examples include investigations of localized biochemistry in larger cells [9], anatomical studies of multi-cellular organisms or

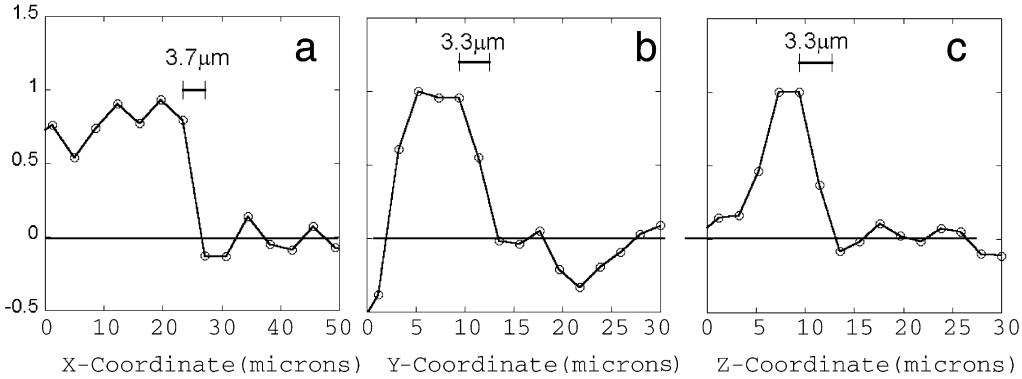

Fig. 5. Panel (a) is a magnified view of signal vs. X over the 50 μm region labeled in Fig. 4a. The edge feature shows a drop from full intensity to zero over a width of 3.7 μm, confirming the expected 3.7 μm resolution. Panels (b) and (c) are analogous plots of signal vs. Y and Z over the regions labeled in Fig. 4b and c, and confirm the expected resolution of 3.3 μm in those directions.

embryos [19], and histological studies of tissues, including brain. [20].

5. Experimental

MRI microscopy images of Fig. 3 are taken at room temperature at a field of 9 T (383 MHz), using phase encoding for all three spatial directions [14,15]. An initial 90° pulse is followed by application of phase-encoding gradient pulses along the X (Y) [Z] axes of duration 925 μs (800 μs) [800 μs] and amplitudes ranging over ±4.6 T/m (±5.8 T/m) [±5.8 T/m] in 64 (20) [20] steps. These values determine the "nominal" resolution along X (Y) [Z] to be 3.7 μm (3.3 μm) [3.3 μm]. The corresponding field-of-view is 237 μm (66 μm) [66 μm].

The constant-time-imaging sequence employed sidesteps complications associated with susceptibility broadening (because it is based on echo amplitude) and T_2 (because the spacing between the 90° and 180° pulses is held fixed). Therefore, if we neglect molecular diffusion during the gradient pulses, and if we can obtain adequate signal-to-noise, then we expect that the true resolution will match the "nominal" resolution listed above. During the short duration of the phase-encoding pulses (made possible by the large gradient strengths) the rms molecular diffusion distance (∼2 μm) is less than the nominal resolutions (∼3–4 μm). (It is also straightforward, with our gradient setup, to increase the gradient strengths and shorten the phase-encoding pulses by as much as a factor of 10.) Therefore, one expects, and confirms from Fig. 5, that the "nominal" resolution quoted above will be realized.

Following phase encoding, a train of 180° pulses is applied to form a Carr–Purcell (CP) or Carr–Purcell–Meiboom–Gill (CPMG) echo train of 256 echoes, with phasing of the rf pulses and the acquisition following the "Phase Alternating-Phase Shift Pulse Sequence (PHAPS)" scheme to remove mirror images [21–24]. The acquisition time for each echo is 512 μs, much less than $T_2^* \sim 1.6$ ms. During acquisition the oscillator frequency is set such that the signal frequency is offset by $(1/512\,\mu s)$. The 256 echoes, each with 32 data points acquired, are then linked to form a one-dimensional array of 8192 points, thereby forming a time domain signal characterized by a decay time $T_2 \sim 50$ ms for the decay of the CP and CPMG envelope, and a correspondingly narrow bandwidth of $(1/(\pi T_2)) \sim 6$ Hz. This array is Fourier transformed, and essentially all of the intensity is observed in the peak at frequency $(1/512\,\mu s)$. (This procedure is analogous to the effect of "spinning sidebands." Here the effective "sidebands" are spaced by a frequency $(1/512\,\mu s)$, much greater than $1/\pi T_2^* \sim 200$ Hz, and so no intensity is found in the sidebands.) For each set of phase encode amplitudes this peak intensity becomes a single element of a $(64 \times 20 \times 20)$ matrix. That array is "zero-filled" to $(64 \times 32 \times 32)$ and fast Fourier transformed to form the image.

Acknowledgments

The authors thank Doug Morris for helpful discussions and advice. This work was supported by the National Science Foundation NSF/DBI9987079.

References

[1] P.T. Callaghan, Principles of Nuclear Magnetic Resonance Microscopy, Clarendon Press, Oxford, 1991.
[2] J.B. Aguayo, S.J. Blackband, J. Schoeniger, M.A. Mattingly, M. Hintermann, Nuclear magnetic resonance imaging of a single cell, Nature 322 (1986) 190–191.
[3] X. Zhou, C.S. Potter, P.C. Lauterbur, B.W. Both, NMR imaging with $(6.37\,\mu m)^3$ isotropic resolution, in: Society of Magnetic

Resonance in Medicine 8th Annual Meeting, Amsterdam, 1989, p. 128.
[4] Z. Cho, C. Ahn, S. Juh, J. Jo, R. Friedenberg, S. Fraser, R. Jacobs, Recent progress in NMR microscopy toward cellualr imaging, Trans. R. Soc. London 333 (1990) 469–475.
[5] Z. Cho, C. Ahn, S. Juh, K. Lee, R. Jacobs, S. Lee, J. Yi, J. Jo, Nuclear magnetic resonance microscopy with 4-μm resolution: theoretical study and experimental results, Med. Phys. 15 (1988) 815–824.
[6] S.-C. Lee, K. Kim, J. Kim, S. Lee, J. Yi, S. Kim, K. Ha, C. Cheong, One micrometer resolution NMR microscopy, J. Magn. Res. 150 (2001) 207–213.
[7] S.C. Grant, D.L. Buckley, S. Gibbs, A.G. Webb, S.J. Blackband, NMR spectroscopy of single neurons, Magn. Reson. Med. 44 (2000) 19–22.
[8] S.C. Grant, D.L. Buckley, S. Gibbs, A.G. Webb, S.J. Blackband, MR microscopy of multicomponent diffusion in single neurons, Magn. Reson. Med. 46 (2001) 1107–1112.
[9] K.R. Minard, R.A. Wind, Picoliter 1 h NMR spectroscopy, J. Magn. Res. 154 (2002) 336–343.
[10] A.G. Webb, Radiofrequency micro-coils in magnetic resonance, Progr. Nucl. Magn. Reson. Spectrosc. 31 (1997) 1–42.
[11] D.A. Seeber, R.L. Cooper, L. Ciobanu, C.H. Pennington, Design and testing of high sensitivity micro-receiver coil apparatus for nuclear magnetic resonance and imaging, Rev. Sci. Instrum. 72 (2001) 2171.
[12] D. Seeber, J. Hoftiezer, W. Daniel, M. Rutgers, C. Pennington, Tri-axial magnetic field gradient system for micro-coil magnetic resonance imaging, Rev. Sci. Instrum. 71 (November) (2000) 4263–4272.
[13] D. Seeber, J. Hoftiezer, C. Pennington, Pin diode-based duplexer for micro-coil NMR, Rev. Sci. Instrum. 71 (7) (2000) 2908–2913.
[14] S. Gravina, D.G. Cory, Sensitivity and resolution of constant-time-imaging, J. Magn. Reson. B 104 (1994) 53–61.
[15] S. Choi, X.-W. Tang, D.G. Cory, Constant-time-imaging approaches to NMR microscopy, Int. J. Imaging Syst. Technol. 8 (1997) 263–276.
[16] Commenting on the resolution standard used, we note that one can obtain the effective "point spread function" characterizing the resolution of an imaging system by differentiating the observed signal over the region of an edge feature in the phantom. So a drop-off from 100% signal strength to 0 over one voxel width implies a point spread function having width equal to one voxel width. This resolution standard based on width of edge features is convenient for imaging and commonly used (see e.g., [6]).
[17] A. Schaff, W. Veeman, Mechanically detected nuclear magnetic resonance at room temperature and normal pressure, J. Magn. Res. 126 (1997) 200–206.
[18] A. Webb, S. Grant, Signal-to-noise and magnetic susceptibility trade-offs in solenoidal micro-coils for NMR, J. Magn. Reson. B 113 (1996) 83–87.
[19] A.Y. Louie, M.M. Huber, E.T. Ahrens, U. Rothbacher, R. Moats, R.E. Jacobs, S.E. Fraser, T.J. Meade, In vivo visualization of gene expression using magnetic resonance imaging, Nat. Biotechnol. 18 (2000) 321–325.
[20] C.T. Huesgen, P.C. Burger, B.J. Crain, G.A. Johnson, In vitro MR microscopy of the hippocampus in Alzheimer's disease, Neurology 43 (1993) 145–152.
[21] R. Graumann, A. Oppelt, E. Stetter, Multiple spin-echo imaging with a 2D fourier method, Magn. Reson. Med. 3 (1986) 707–721.
[22] J. Hennig, Multiecho imaging sequences with low re-focusing flip angles, J. Magn. Reson. 78 (1988) 397–407.
[23] L.P. Panych, R.V. Mulkern, P. Saiviroonporn, Non-fourier encoding with multiple spin echoes, Magn. Reson. Med. 38 (1997) 964–973.
[24] Y. Zur, S. Stokar, A phase cycling technique for canceling spurious echoes in NMR imaging, J. Magn. Reson. 71 (1987) 212–228.